Hydrogen-related defects in polycrystalline CVD diamond

X. Zhou and G. D. Watkins
Department of Physics, Lehigh University, Bethlehem, Pennsylvania 18015

K. M. McNamara Rutledge* and R. P. Messmer
General Electric Corporate Research and Development, Schenectady, New York 12301

Sanjay Chawla†
Department of Physics, University of Pennsylvania, Philadelphia, Pennsylvania 19104
(Received 22 May 1996)

By simulating the line shapes of a commonly observed $S=1/2$ electron paramagnetic resonance (EPR) center in polycrystalline chemical vapor deposited (CVD) diamond at 9.8, 14, 20, and 35 GHz, we conclude that the EPR signal, which we label H1, results from a *unique* defect with a single hydrogen atom ~ 1.9 Å away from the unpaired electronic spin. We report also 14 and 20 GHz studies of an additional hydrogen-related EPR center, labeled H2, which is similar; however, the hydrogen is ~ 2.3 Å away. We propose that, in each case, a hydrogen atom has entered a stretched bond at a grain boundary or other extended misfit region in the CVD material, allowing the carbons to relax backward, one bonding to the hydrogen, the other with an unpaired electron in its dangling bond. These results may provide important insight into the recently discovered phenomenon of hydrogen *activation* at grain boundaries in silicon. [S0163-1829(96)04236-1]

I. INTRODUCTION

There is considerable current interest in polycrystalline chemical vapor deposited (CVD) diamond films for possible high temperature semiconductor applications, as well as for applications using their high mechanical strength and thermal conductivity. Critical to their potential as semiconductors is the ability to passivate the many grain boundaries, surfaces, and other imperfections in such films, hopefully accomplished by the large concentration of hydrogen present in the processing. In this paper we describe an electron paramagnetic resonance (EPR) study of a variety of such samples. We report two apparently distinct hydrogen-related EPR signals in such films, which reveal that electrically active centers involving hydrogen remain.

One, which we label H1, has been reported by several workers in spectrometers operating at ~ 9 GHz,[1–4] and is characterized by a signal at $g=2.0028$ with a weak pair of partially resolved satellites, which were established to arise from hyperfine interaction with hydrogen.[3] From observation of a variation in satellite intensities and positions when observed at 35 GHz, it has been further suggested that they arise from ''forbidden'' $\Delta m=\pm 1$ nuclear spin flips of the hydrogen nucleus during the EPR $\Delta M=\pm 1$ transitions.[4] In the present paper, we report studies of this center at the intermediate frequencies 14 GHz and 20 GHz, which confirm unambiguously the $\Delta m=\pm 1$ origin of the satellites. In addition, we demonstrate the remarkable result that we can match the relative intensities of the central and satellite components as well as the overall line shapes at all four frequencies by the assumption of a single *unique* defect with a well-defined hyperfine interaction arising from a single hydrogen atom.

The second defect, not previously reported, is seen in only a few samples, where H1 is absent. We label it H2. It is similar to H1, being centered again at $g=2.0028$, but it is narrower, allowing its satellites, which are a factor of ~ 2–3 less intense compared to the central line, to be better resolved. We find that a good fit to the satellite intensities and the overall line shapes for it can again be made by assuming a single unique defect but with hyperfine interaction with a single hydrogen $\sim 60\%$ of that for H1.

In the following, we demonstrate that the relative intensity of the satellites and the central line depends primarily on the anisotropic part of the hyperfine interaction, which, in turn, supplies an estimate of the distance between electron spin and hydrogen atom. From this we estimate ~ 1.9 Å for H1 and ~ 2.3 Å for H2, each being between the nearest carbon-carbon distance in diamond (1.54 Å) and the next nearest distance (2.51 Å). They are therefore close to what one might expect for the distance between a dangling bond on one neighbor of a vacancy and a hydrogen atom terminating the dangling bond on another of its neighbors, suggesting single hydrogen atoms in vacancylike stretched bonds at grain boundaries or other extended misfit regions in the polycrystalline materials.

The outline of the paper is as follows. In Sec. II we describe the experimental details, and in Sec. III the experimental results. In Sec. IV the theory for the intensities and positions of forbidden $\Delta m=\pm 1$ transitions is outlined and the experimental results analyzed. In Sec. V models for the defects are presented and discussed, and compared to a theoretical treatment for a single hydrogen atom in a vacancy. In Sec. VI a summary is presented.

II. EXPERIMENTAL DETAILS

The samples were produced by a proprietary chemical vapor deposition technique using a subatmospheric microwave plasma of hydrogen with low concentrations of gas-

TABLE I. Samples studied, with estimated concentrations of the defects giving rise to the H1, H2, and N^0 EPR signals, and total concentrations of hydrogen (determined by NMR) and nitrogen and oxygen (determined by combustion analysis), where available.

Sample	H1 (10^{16} cm^{-3})	H2 (10^{16} cm^{-3})	N^0 (10^{16} cm^{-3})	[H] (at. %)	[N] (at. %)	[O] (at. %)
1153	0	3.2	14	0.021	0.005	0.009
1188	0	4.8	24	0.027	0.002	0.005
1184	0	$\leqslant$0.4	24		0.009	
1246	0	$\leqslant$0.5	5			
1192	$\leqslant$3	0	30			
1204	50	0	11			
1267	16	0	12	0.045	0.004	0.016
1146	$\leqslant$6	0	18	0.085	0.002	0.003
1242	67	0	1.3	0.15	0.004	
1431	111	0	5			
1227	119	0	0	0.29		
1171	92	0	1.5	0.32	0.007	0.029
1175	78	0	0	0.33	0.011	0.052

eous carbon-containing species, and in some cases, oxygen. The samples were free standing, 100–500 μm thick, after silicon substrate removal and were cleaned in acid before study. Nitrogen was not added intentionally as a component of the gas phase but was present as a result of bottled gas impurities and minor vacuum leaks. The samples studied are listed in Table I. Where available, hydrogen concentration determined by NMR, and nitrogen and oxygen concentrations determined by combustion analysis, of representative samples from each wafer are included.

The EPR spectra were observed at room temperature in absorption, using balanced bolometer spectrometers operating at 14 and 20 GHz. Low microwave power ($\sim$5 μW) and magnetic field modulation amplitude ($\sim$0.5 G peak to peak) were used to avoid saturation and line shape distortion, respectively. Where necessary, digital signal averaging was performed by repeated sweeps through the resonance, to improve signal to noise. Defect concentrations were determined by double integration of their derivative 14 GHz EPR spectra, corrected for the microwave power, magnetic field modulation, and sample volume, and compared to that of a 0.4 mg (10^{18} spins) reference sample of $CuSO_4 \cdot 5H_2O$. We estimate the accuracy of the absolute concentration estimates to be within a factor of 4.

For annealing studies, the sample was placed in a quartz tube and inserted for 30 min into a horizontal tube furnace, preset at the desired temperature, and then withdrawn. For temperatures above 900 °C, the tube was maintained under vacuum.

III. RESULTS

In Fig. 1 we show the EPR spectra at 14 GHz for two representative samples. In Fig. 1(a), the spectrum of sample 1175 reveals the H1 spectrum previously reported by several groups.[1–4] It is characterized by a single line at $g=2.0028$ with a partially resolved pair of weaker satellites on either side. No other resonances are observed. In Fig. 1(b), the spectrum of sample 1153 reveals the strong polycrystalline pattern spectrum of isolated neutral substitutional nitrogen[5] ($g=2.0023$, $A_{\parallel}=114.0$ MHz, $A_{\perp}=81.3$ MHz) plus a weaker signal with satellites, which is centered at somewhat lower field than the central nitrogen signal, at $g=2.0028$. This is the spectrum we label H2.

In Table I we list concentration estimates of the defects giving rise to the three EPR signals found in the various

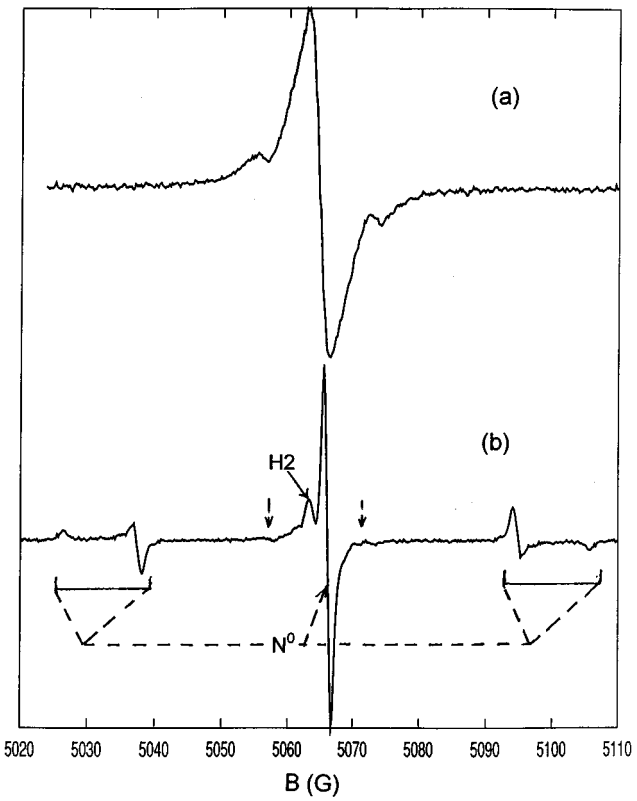

FIG. 1. EPR spectra at 14 GHz of (a) sample 1175, showing the H1 spectrum, and (b) sample 1153, showing the strong powder pattern spectrum of N^0, plus the weaker H2 spectrum centered at slightly lower field.

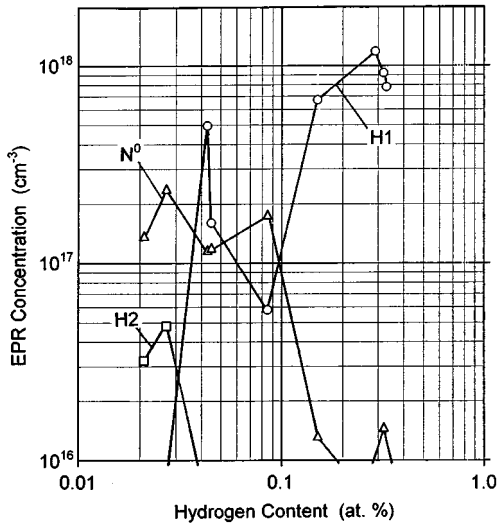

FIG. 2. Concentrations of the defects giving rise to the H1, H2, and N^0 EPR spectra vs hydrogen content determined by NMR.

samples. We note that there appears little correlation between the strength of the N^0 signal and the nitrogen concentration. There is, however, a suggestive pattern for the three spectra vs hydrogen concentration, which is shown in Fig. 2. There, an anticorrelation between the N^0 and H1 spectra is suggested, the N^0 spectrum observed primarily with H content below $\sim 0.1\%$, the H1 spectrum, above. H2 is seen only in the lowest hydrogen-containing samples.

A. The H1 spectrum

In Fig. 3 we show the H1 spectrum on an expanded scale at 14 and 20 GHz, along with the results taken from Fig. 1 of Holder, Rowan, and Krebs[4] at 9.8 and 35 GHz. Taken together they clearly show a monotonically increasing separation and decreasing intensity for the satellites as the microwave frequency is increased. That this is the characteristic behavior for forbidden $\Delta m = \pm 1$ nuclear spin flips will be confirmed in Sec. IV, where the theory is presented.

In Fig. 4(a) we show the microwave power dependence at 20 GHz of the central and satellite resonances. Similar behavior is observed at 14 GHz. Plotted on a log-log plot vs the square root of microwave power (i.e., $\sim H_1$), the linear behavior of the central component followed by the onset of flattening at higher power, without broadening of the resonance, is characteristic of saturation for an inhomogeneously broadened line.[6] The satellites, however, show only slight evidence of saturation at the highest power available in the figure. This points up the necessity of making the measurements at low microwave power in order to obtain an undistorted spectrum reflecting the true relative intensities of satellite and central components. The 14 and 20 GHz spectra of Fig. 3 were performed at $<5\mu$W $[H_1/(H_1)_{\max}=0.06$ in Fig. 4(a)] to assure compliance. The reason for this unusual difference in saturation behavior for different lines associated with the same spectrum will be clarified also in Sec. IV.

Isochronal annealing studies in 100 °C intervals confirm the earlier results of Jia *et al.*,[3] of no significant loss of the defect until ~ 1500 °C. A careful study of the spectrum after each anneal revealed no change as well in its shape or width.

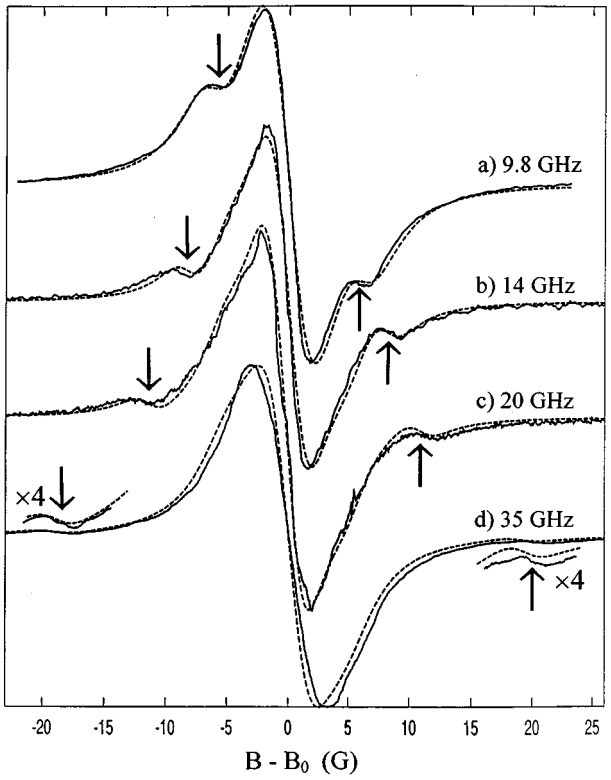

FIG. 3. EPR spectra of H1 (solid lines) at four different microwave frequencies ν, centered in each case around $B_0 = h\nu/g\mu_B$. The satellite positions are indicated by arrows. Also shown (dashed lines) are the theoretical fits. (The experimental spectra at 9.8 and 35 GHz have been taken from Ref. 4.)

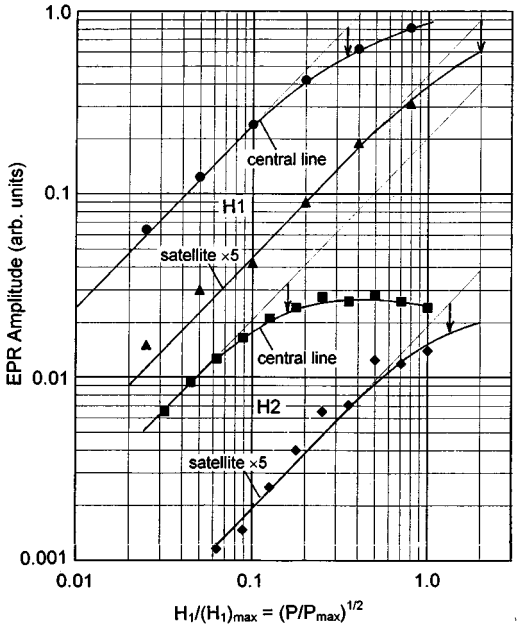

FIG. 4. Saturation properties of the central line and satellites at 20 GHz vs microwave magnetic field in the cavity (H_1) for (a) H1, and (b) H2. The saturation points (see text) are indicated by the arrows.

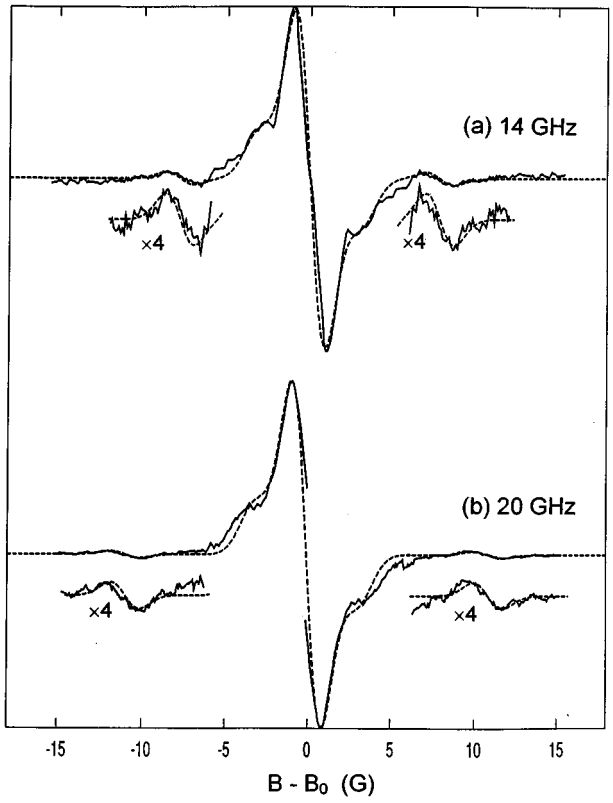

FIG. 5. EPR spectra of H2 at 14 and 20 GHz, centered around $B_0 = h\nu/g\mu_B$. Also shown (dashed lines) are the theoretical fits.

B. The H2 spectrum

The H2 spectrum is shown on an expanded scale in Fig. 5 at 14 and 20 GHz. By comparison with Figs. 3(b) and 3(c), it is clear that the lines are less broad and the satellites, although weaker, are much better resolved than for H1.

These spectra were obtained in the following way. (i) The intensity of H2 was considerably weaker than H1, and at the low microwave power required for nonsaturation of the signals, the signal to noise was very poor. As a result, substantial signal averaging ($\sim$200 sweeps) was employed. In addition, evidence of preferential orientation of the crystal grains in the particular two samples displaying this signal was evident by subtle changes in the polycrystalline line shape of the hyperfine split N^0 lines vs magnetic field orientation, as well as in the partially resolved structure evident on the shoulders of the H2 central component. To eliminate this effect, and produce a closer simulation to the real random grain orientation spectrum, the 200 sweeps were divided equally over a full 180° magnetic field orientation in 15° intervals. (ii) The strong interfering central component of the nitrogen signal had to be removed. To accomplish this, the different saturation behaviors of the nitrogen and H2 spectra allowed the subtraction of suitably weighted spectra taken at two different microwave powers to remove most of the nitrogen signal. This separation was most successful on the low field side of the N^0 resonance, made easier by the different g values of the two spectra [see Fig. 1(b)]. As a result, only the the low field side was retained and the high field side shown in the figures has been constructed by inversion through the center. (iii) To improve the satellite signals for the 20 GHz spectrum, they were taken at an increase of microwave power by 12 dB (factor of 4 increase in H_1), still in their nonsaturated regime, and reduced by a factor of 4 in the plot of Fig. 5(b).

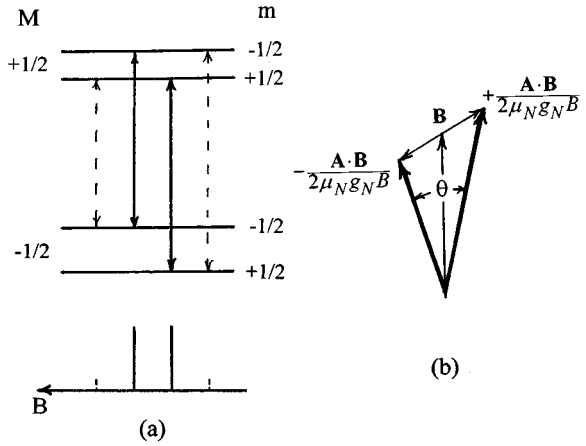

FIG. 6. (a) Energy level diagram and EPR transitions for an $S = 1/2$ electron spin coupled to an $I = 1/2$ nucleus. (b) The effective magnetic field at the nucleus for the two M states.

The saturation behavior of the central and satellite components of H2 is shown in Fig. 4(b). They display the same general behavior as H1 with the exception that saturation occurs at lower power.

IV. THEORY AND ANALYSIS OF THE SPECTRA

The spin Hamiltonian for an electronic spin $S = 1/2$ with isotropic g, coupled to a nuclear spin $I = 1/2$, is

$$\mathcal{H} = g\mu_B \mathbf{S}\cdot\mathbf{B} + \mathbf{S}\cdot\mathbf{A}\cdot\mathbf{I} - g_N\mu_N \mathbf{I}\cdot\mathbf{B}. \tag{1}$$

This leads to four energy levels associated with the $M = \pm 1/2$ and $m = \pm 1/2$ states, as illustrated in Fig. 6(a), with the normally allowed $\Delta m = 0$ and forbidden $\Delta m = \pm 1$ transitions as indicated. Consider now the nuclear part of the above Hamiltonian, which to first order in $A/g\mu_B B$ becomes

$$\mathcal{H}_N = -g_N\mu_N \mathbf{I}\cdot\left(\mathbf{B} - \frac{\mathbf{A}\cdot\mathbf{B}M}{g_N\mu_N B}\right). \tag{2}$$

Here g and g_N are the electronic and nuclear g values, respectively, μ_B and μ_N the corresponding Bohr magnetons, **S** and **I** the corresponding spin operators, **A** the nuclear hyperfine tensor, and $M = \pm 1/2$ is the azimuthal quantum number for **S** quantized along **B**, the applied magnetic field. The bracketed term represents an effective magnetic field at the nucleus, and when **A** is anisotropic, its two vector components **B** and $\pm\mathbf{A}\cdot\mathbf{B}/2g_N\mu_N B$ can point in different directions, as illustrated schematically in Fig. 6(b). Thus the quantization axis for the nucleus differs for the two M quantization states, and destroys as a consequence the orthogonality of the $m = \pm 1/2$ nuclear quantization states between the two. The intensity of the EPR transitions is proportional to

$$I\left(+\frac{1}{2},m\leftrightarrow-\frac{1}{2},m'\right)\propto\left|\left\langle+\frac{1}{2}\left|S_+\right|-\frac{1}{2}\right\rangle\right|^2|\langle m|m'\rangle|^2H_1^2, \tag{3}$$

where $|\langle m|m'\rangle|^2=\cos^2(\theta/2)$ for the $\Delta m=0$ transitions and $\sin^2(\theta/2)$ for the $\Delta m=\pm1$ transitions, θ is the angle between the nuclear quantization axis for $M=+1/2$ ($\mathbf{B}-\mathbf{A}\cdot\mathbf{B}/2g_N\mu_NB$) and that for $M=-1/2$ ($\mathbf{B}+\mathbf{A}\cdot\mathbf{B}/2g_N\mu_NB$), and H_1 is amplitude of the microwave magnetic field. As illustrated in the figure, θ can depart substantially from zero when the anisotropy in $\mathbf{A}\sim2g_N\mu_NB$, leading to significant intensity in the forbidden $\Delta m=\pm1$ transitions.[4,7,8]

From this, the general dependence of the H1 satellites in Fig. 3 is immediately explained. As B increases, θ decreases as B^{-1}, the forbidden intensities decrease, therefore, as B^{-2}, where $B\approx B_0=h\nu/g\mu_B$, and the satellite positions, given by Eq. (1), approach field values of $\pm(g_N\mu_N/g\mu_B)B_0$ to either side of the central line.

We now take the approach a step further and attempt to simulate the detailed shapes of the H1 spectra using the theory above, and the assumption that a single hydrogen atom is involved. We assume axial symmetry for **A**, which, for any angle ϕ between the symmetry axis and **B**, gives four lines, as illustrated in Fig. 6(a), two for the $\Delta m=0$ transitions, and two for the $\Delta m=\pm1$, whose intensities are given by Eq. (3). We convolute these with a random distribution function for the defect axis orientation, $N(\phi)d\phi=\frac{1}{2}\sin\phi d\phi$, and then convolute again with the derivative of a Lorentzian line shape vs B. There are thus only three adjustable parameters, $A_{||}$, $A_\perp$ (or, the isotropic part $a=\{A_{||}+2A_\perp\}/3$, the anisotropic part $b=\{A_{||}-A_\perp\}/3$), and the Lorentzian linewidth, which must give a good fit to the experimental derivative spectra at all four microwave frequencies.

In Fig. 7 we illustrate the fitting process for the 20 GHz results and in Fig. 3 we show the fit for all four frequencies using the values of $a=5.5$ MHz and $b=11.0$ MHz. The Lorentzian used for the best match shown in the figure for the sample used in our 14 and 20 GHz results had a peak-to-peak derivative width (PPDW) equal to 2.8 G. For the sample used by Holder, Rowan, and Krebs[4] at 9.8 and 35 GHz, the PPDW was taken to be 3.6 G. Studies reported in previous reports display different degrees of resolution of the satellites consistent with sample-dependent breadth differences,[1–4] and such an adjustment, which is one of resolution only, is therefore appropriate. By adjusting a and b, we conclude that the excellent fit to H1 at all four frequencies shown in the figure requires $b=+11.0$ MHz and $a=+5.5$ MHz, with an uncertainty of $\pm$ 2.5 MHz for each. (We have tested the effect of departures from axial symmetry by introducing an additional parameter b', such that $A_\parallel=A_1=a+2b$ remains the same but $A_\perp$ is replaced by two orthogonal components $A_2=a-b-b'$ and $A_3=a-b+b'$. Keeping $a=5.5$ MHz and $b=11.0$ MHz, significant departures from the predicted line shapes are observed only for $|b'|\geqslant5$ MHz, i.e., $\frac{1}{2}|A_3-A_2|=|b'|\geqslant0.4|b|$, which represents a reasonable boundary for acceptance. We conclude that the predicted shape is insensitive to modest departures from axial symmetry.)

The relative intensities of the satellites are determined primarily by the anisotropic part of the hyperfine interaction b, i.e., $\sim b^2$. This is illustrated in Fig. 8, which includes also

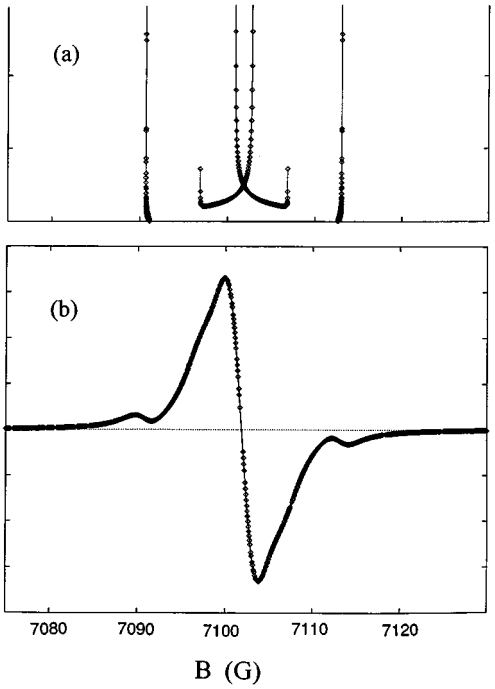

FIG. 7. (a) Predicted polycrystalline pattern for H1 at 20 GHz using $a=+5.5$ MHz and $b=+11.0$ MHz. (b) Predicted EPR spectrum after convolution with the derivative of a Lorentzian with 2.8 G PPDW.

the positions deduced above for the H1 spectra at the four frequencies. On the other hand, the shape of the central line, which arises from the normally allowed hyperfine structure, depends strongly on the ratio of a to b, as indicated in Fig. 7(a). Because of this, the range of values for b and a beyond which a satisfactory fit to the H1 spectra cannot be obtained

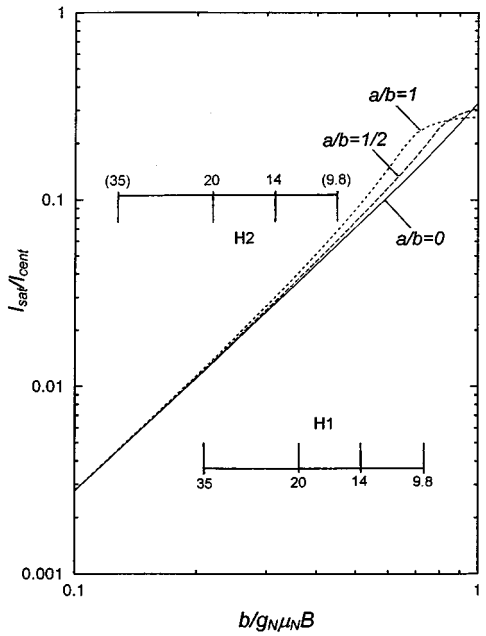

FIG. 8. Dependence of the satellites-to-central-component intensity ratio on the hyperfine parameters a and b.

is so narrowly defined. The absolute signs of a and b cannot be determined but have been taken as those appropriate for dipole-dipole origin of the anisotropy, see below.

A similar treatment for the H2 spectrum has also been performed, and the results are shown by the dashed lines in Fig. 5. In this case, $a=4.5$ MHz and $b=6.7$ MHz, and convolution with the derivative of a *Gaussian* with full width at half maximum (FWHM) of 2.0 G gives the best fit. With the exception of the weaker partially resolved structure on the shoulders of the central line, the relative intensity of the satellites and the general shape of the central component are successfully reproduced. (The shoulder structure could be evidence of departures from axial symmetry for **A** not included in our treatment, or incomplete angular averaging associated with preferred grain orientations out of the magnetic field plane.) We estimate the uncertainty in the value for a to be ± 2.0 MHz and for b, ± 1.5 MHz, outside of which the match to the spectra is unacceptable.

The different saturation behavior for the central vs satellite components of each spectrum also follows naturally from the theory. As pointed out in Sec. III, the saturation behavior of Fig. 4 is characteristic of inhomogeneously broadened lines,[6] as expected in this case because of angular averaging over the differently oriented crystalline grains, Fig. 7(a), plus the additional Lorentzian or Gaussian broadening associated presumably with more distant hydrogen hyperfine interactions. For such a system, with $S=1/2$, the signal intensity is $1/\sqrt{2}$ of the saturation value when $2WT_1=1$, where W is the microwave induced $\Delta M=\pm 1$ transition rate and T_1 is the effective spin-lattice relaxation time between the two levels involved in the transition. From Eq. (3), $W(\Delta m=0) \propto H_1^2\cos^2(\theta/2)$ and $W(\Delta m=\pm 1)\propto H_1^2\sin^2(\theta/2)$ at a particular defect, and, assuming the same T_1 and spin packet width for the allowed and forbidden transitions, the ratio of their saturation values for H_1^2 would therefore be given by

$$\frac{[H_1^2(\Delta m=0)]_{\rm sat}}{[H_1^2(\Delta m=\pm 1)]_{\rm cent}}=\frac{\left\langle \cos^2\frac{\theta}{2}\right\rangle}{\left\langle \sin^2\frac{\theta}{2}\right\rangle}=\frac{I_{\rm cent}}{I_{\rm sat}}, \tag{4}$$

where $\langle\ \rangle$ denotes the angular average over all crystalline grain orientations, and $I_{\rm sat}$ and $I_{\rm cent}$ are the unsaturated integrated intensities of the satellites and central components, respectively. The saturation curves shown for the satellites in Fig. 4 have been drawn by displacing the central line curves by $\sqrt{I_{\rm cent}/I_{\rm sat}}$, as determined from Fig. 8 at 20 GHz for each of the H1 and H2 spectra. The agreement with the experimental results is good, serving as an additional confirmation of the forbidden origin of the satellites.

V. DISCUSSION

The narrow allowable range of the hyperfine parameters for the two resonances suggests that each results from a well-defined defect involving a single hydrogen. The isotropic part of the hyperfine interaction a in each case is small, being only a few tenths of a percent of that for atomic hydrogen (1420 MHz), so that, for each, the hydrogen atom must be considered only a neighbor of the paramagnetic site. We treat therefore the anisotropic term b as arising from dipole-dipole interaction between separated electronic and nuclear dipoles, $b=g\mu_B g_N\mu_N/r^3$, which gives the effective separation for H1, $r=1.9$ Å, and for H2, $r=2.3$ Å (and determines the sign of b to be positive). This is an interesting result. The hydrogen atom is very close, these distances being between the nearest C-C diamond lattice separation, 1.5 Å, and the next nearest separation, 2.51 Å. (A check as to whether this simple dipole-dipole model is appropriate for such close separations is afforded by the results for bond-centered muonium in diamond.[9] There, $b=186.9$ MHz, and the dipole-dipole expression, with $g_N=17.708$, predicts $r=1.1$ Å , remarkably close even in this extreme case to that expected for the C-H distance.)

These distances are similar to what one might expect for the distance between a carbon atom next to a lattice vacancy and a hydrogen atom bonded to one of the other carbon neighbors of the vacancy (1.74 Å with a typical C-H bond distance of 1.09 Å, and the carbon atoms in their normal unrelaxed lattice sites; upon breaking the weak next-nearest-neighbor reconstructed bonds at the vacancy, significant relaxation backward should occur, increasing this distance). Many vacancylike sites are expected in such polycrystalline films — in the bulk, at dislocation cores, but particularly at or near the many grain boundaries, which, of necessity, contain vacancylike reconstructed bonds adjacent to the extra atom planes that support the angle between the lattice planes of the adjacent grains. Such stretched bonds are vulnerable to single hydrogen atoms which can enter and break them, attaching to one of the carbon atoms, and activating a vacancylike dangling bond on the other as the two relax backward. If we had a hydrogen atom in an *isolated* bulk vacancy, we would expect easy hopping of the dangling bond among the three remaining carbon neighbors as well as motion of the hydrogen itself, as is commonly observed for such defects.[10–12] For either center, however, no such effects are observed from 1.5 K to room temperature, and we conclude therefore that here we are dealing with highly distorted vacancylike defects, such as can occur at grain boundaries, surfaces, or other misfit regions resulting from the CVD growth. Ideally, hydrogen should serve to passivate such regions, but it takes two hydrogens to passivate both partners of a bond. One will not.

In order to obtain a theoretical test for a hydrogen-vacancylike defect, we have carried out cluster calculations to model a single hydrogen atom inside an isolated bulk vacancy (henceforth labeled $\{V,\mathrm{H}_1\}$). The optimized geometries were obtained within the restricted open-shell Hartree-Fock (ROHF) approximation using both semiempirical and *ab initio* methods. The clusters were terminated by hydrogen atoms, placed at 1.09 Å from the outer carbon atoms, in the direction of bulk carbon atoms. Optimized geometries were first obtained from semiempirical Austin model 1 (AM1) Ref. 13 calculations on a 34 carbon atom cluster [which includes up to fourth nearest neighbors (NNs) of the vacant site] terminated by hydrogens, by relaxing the carbon atoms bordering the vacancy (i.e., the NNs) as well as the hydrogen atom inside it (henceforth labeled H_1). The result, shown in Fig. 9, was that H_1 bonds, as expected, to a single neighbor of the vacancy (labeled C_1), two of the remaining C's form a weak stretched pair bond, and the third ($\mathrm{C}_{\rm DB}$) relaxes backward with an unpaired spin in its dangling orbital. The key

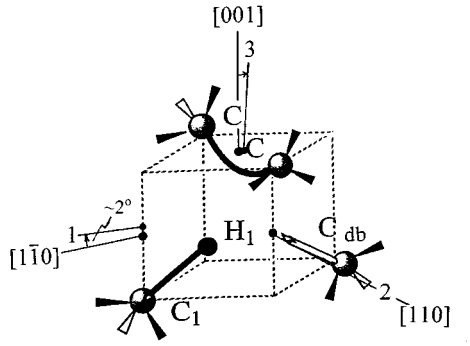

FIG. 9. Model showing the approximate atom positions calculated for $\{V,H_1\}$, a single hydrogen atom in a vacancy, and the principal axes for the hydrogen hyperfine interaction.

geometric parameters obtained are shown in Table II. As expected, the bond between the atom bordering the vacancy C_1, and one of its three back-bonded neighbors, C_{BB}, has decreased in length, while that between the carbon atom with the dangling bond (C_{DB}) and H_1 has increased to 1.95 Å . In order to examine cluster size effects, a larger cluster with 69 carbon atoms (which includes up to sixth NNs) was then modeled, and H_1, the NN as well as next NN (NNN) carbon atoms relaxed. It can be seen that this results in small changes in the local geometry. To assess the reliability of the geometry obtained from the semiempirical calculations, we optimized the positions of the NN carbon atoms and H_1 in a 16 carbon atom cluster (which includes NN and NNN carbon atoms) within the ROHF approximation, using a standard double ζ basis[14] on all the carbon atoms. The NNN positions of carbon atoms were fixed at those obtained from the AM1 geometry obtained from the 69 carbon atom cluster. As seen from the geometry labeled Hartree-Fock(+AM1) in Table II, this results in a shorter C_1-H_1 bond, and a slightly (0.02 Å) greater relaxation of C_{DB}, resulting in a larger C_{DB}-H_1 distance (see table). The shorter C_1 -H_1 bond (by about 3–5%) length compared to C-H bonds in alkanes[15] is typical of Hartree-Fock results, and if taken into account gives a value of 1.94–1.97 Å for the distance between the dangling bond and the hydrogen nucleus. Given expected errors of up to ~0.1 Å , it can be seen that the calculated C_{DB}-H_1 distance is in reasonable agreement with the estimated value of ~ 1.9 Å for the H1 defect, though much smaller than that estimated for the H2 defect.

We have also examined the stability of more than one hydrogen atom inside a vacancy. The optimized hybrid Hartree-Fock(+AM1) geometry of a two-hydrogen vacancy ($\{V,H_2\}$) 16 carbon atom cluster was calculated, and its stability relative to the $\{V,H_1\}$ defect obtained. We find that the former is 2.7 eV less stable than the latter, due to the strong Pauli repulsions between the C-H bond electrons, coupled with the rigidity of the diamond lattice. This result explains why such dangling bond single H-vacancy defects would remain largely unpassivated, even with excess hydrogen present in the growth process of CVD diamonds.

In order to further assess the validity of a H-vacancy model, we have calculated the hyperfine couplings (HFC's) of the paramagnetic $\{V,H_1\}$ complex. The isotropic couplings were obtained by evaluating the spin density at the hydrogen nucleus, while the anisotropic couplings were evaluated by averaging the electron-dipole–nuclear-dipole interaction over the spin distribution. To estimate changes in the couplings due to choice of geometry, the HFC's have been calculated at both the AM1 (69 carbon atom) and hybrid Hartree-Fock(+AM1) geometries. In addition, in order to include spin polarization contributions, the results were obtained with a small H_3C_1-H_1-$C_{DB}H_3$ cluster (with the C_1, C_{DB}, and H_1 atoms at their optimized positions) at various levels of approximation — ROHF, multiconfiguration-(MC) self-consistent field (SCF), and MC-based perturbation theory[16] (PT), using a double ζ basis with additional polarization functions. Polarization contributions were obtained from the C_1-H_1 bonding orbital, as well as the neighboring six C-H orbitals, the former being obtained from a variational MC-SCF calculation, and the latter from a perturbative calculation. We find that these contributions resulted in an increase in the anisotropic HFC's by 10–15 %, with much larger percentage changes in the isotropic couplings. Hartree-Fock calculations with a larger $(H_3C)_3C_1$-H_1-$C_{DB}(CH_3)_3$ cluster resulted in changes of less than 3% compared to those with the smaller cluster, suggesting small cluster size effects on the HFC's. The results from calculations with the small cluster from the MC-based PT are listed in Table III. It can be seen from the table that the isotropic couplings a are small [~1% of that for atomic hydrogen (1420 MHz)], and in reasonable agreement with experiment (about 0.4% of atomic hydrogen value). The strong dependence of the isotropic couplings on geometry is typical of systems with spin polarization effects.[17] As can be seen by comparison between the HFC's at the AM1 and Hartree-Fock geometries, the anisotropic couplings are much less sensitive to geometry. Note that the hyperfine interaction departs from axial symmetry, i.e., $\frac{1}{2}(A_3-A_2)=b'\neq 0$, as expected when averaging over the spatial extent of the dangling bond spin. The principal 1,2,3 axes are indicated in Fig. 9. However, the departure is small, according to the criterion developed in the preceding section. Approximating, therefore, the defect to be axially symmetric gives $b\approx(A_1-a)/2$, which, from Table III, is 8.9–9.5 MHz. These values are between the experimental estimates for H1 (11.0 ± 2.5 MHz) and H2 (6.7 ± 1.5 MHz), but closest to H1, being within the experimental

TABLE II. Geometric parameters of the $\{V,H_1\}$ complex.

Cluster	Method	C_{DB}-H_1	C_1-H_1	C_1-C_{DB}
Unrelaxed		1.74 Å	1.09 Å	2.51 Å
34 C atom	AM1	1.95 Å	1.14 Å	2.73 Å
69 C atom	AM1	1.96 Å	1.14 Å	2.77 Å
16 C atom	Hartree-Fock (+AM1)	2.01 Å	1.04 Å	2.79 Å

TABLE III. Hyperfine coupling constants (in MHz) of the $\{V,H_1\}$ complex. Experimental values for the H1 and H2 defects (assumed to have axial symmetry) are included for comparison.

Geometry	C_{DB}-H_1	a	b	$b'=\frac{1}{2}(A_3-A_2)$
		Theory ($\{V,H_1\}$ defect)		
AM1 (69 C atom cluster)	1.96 Å	−12.0	+9.5	+3.5
Hartree-Fock (16 C atom cluster)	2.01 Å	+16.0	+8.9	+1.6
		Experiment		
H1 defect	~1.9 Å	(+)5.0±2.5	(+)11.0±2.5	~0
H2 defect	~2.3 Å	(+)4.0±2.0	(+)6.7±1.5	~0

estimated accuracy for it. This agreement serves as additional justification of our interpretation for H1, and possibly also for H2, as arising from distorted vacancylike defects.

A possible alternative model that we have investigated is that H2 is the real single hydrogen in a vacancylike defect, with $r=2.3$ Å , and that H1 is a similar vacancylike defect but with two or three equivalent hydrogens at the same distance decorating more of the vacancy near neighbors. (With n hydrogens, the satellite intensities should be $\sim n$ times that for a single hydrogen because each hydrogen can be flipped.) Figure 10 shows the result of taking the a and b parameters for H2 and successively convoluting for two or three equivalent hydrogen neighbors, constrained to have their hyperfine axes pointing along different $\langle 111\rangle$ directions, as appropriate for a vacancy, and then convoluted with either the FWHM = 2.0 G Gaussian derivative function found for H2 (dashed lines) or the PPDW = 2.8 G Lorentzian found appropriate for the original match to H1 (dotted lines). It is immediately obvious that neither works, the central line becoming too broad and the satellites also, which is particularly evident when three are involved. The reason for this is clear: The sharpness of the central component is possible for one hydrogen because the angular distribution function $N(\phi)d\phi=\frac{1}{2}\sin\phi d\phi$ strongly weights $A_\perp=(a-b)$, which can be made small by selection of $a\sim b$, where b is independently determined by the amplitude of the satellites. This is not possible as soon as two or more hydrogens with different $\langle 111\rangle$ axes are involved because, when perpendicular to one, the probability that **B** also be perpendicular to the others is vanishingly small for two (proportional to the sine of the angle of **B** with respect to the normal of the plane containing the two $\langle 111\rangle$ hyperfine axes), and zero for three. Substantial hyperfine contributions to the central line breadth proportional to b are therefore unavoidable.

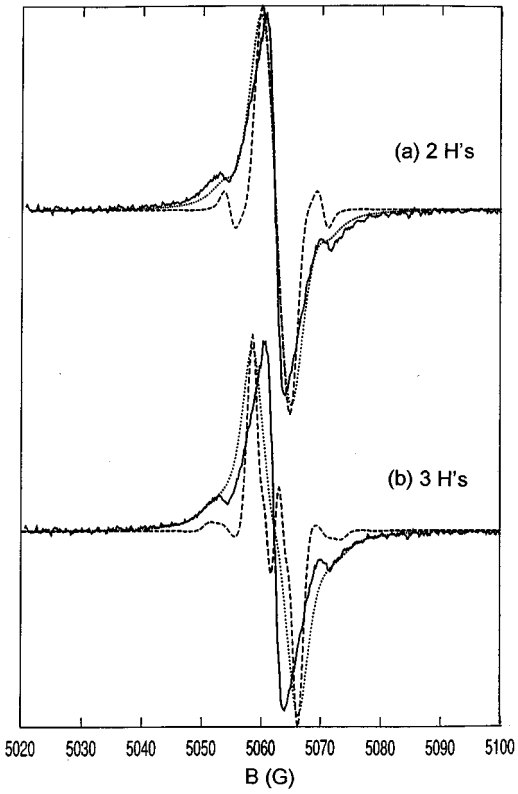

FIG. 10. 14 GHz spectrum predicted (dashed lines for convolution with the derivative of a Gaussian of 2.0 G FWHM, dotted lines for a Lorentzian of 2.8 G PPDW) for a vacancy dangling bond with (a) two, or (b) three hydrogen atoms bonded to the other carbon neighbors of the vacancy, using the single-hydrogen hyperfine parameters of H2. The experimental spectrum for H1 is given by the solid lines.

The H2 spectrum is matched best with a Gaussian width function, while the longer tails evident on H1 are simulated much better with a Lorentzian. Since carbon has only a very low abundance isotope with nuclear magnetic moment (^{13}C, 1.1%), the origin of the width must come from hyperfine interactions with other nearby hydrogens. A random distribution of magnetic nuclei in a three dimensional crystalline lattice leads to Lorentzian line shapes.[18] On the other hand, a regular distribution on a lattice, or interaction with a finite number of close neighbors, tends toward a Gaussian shape.[19] This suggests that the shapes potentially also contain detailed microscopic information regarding the location of the defects in the lattice, and the arrangements of neighbor hydrogens around them, but we are not prepared to speculate on this issue at this time. The substantial widths in either case, however, do reveal that the defects must be located in regions where large concentrations of hydrogen, not associated with paramagnetic dangling bonds, also exist, supplying an argument for location in extended structural defects of some kind. Arguments have been presented from NMR studies that most of the hydrogen is incorporated in extended two dimensional regions such as grain boundaries,[20,21] implying a corresponding argument for the location of these EPR centers there also. (It should be pointed out, however, that in recent NMR studies of CVD samples,[3,22] the ^{13}C nuclear spin relaxation properties were interpreted to indicate nuclear spin diffusion to paramagnetic centers distributed uniformly throughout the bulk. If in their samples H1 was the dominant

center, with negligible N^0, which *is* uniformly distributed in the bulk, a conflict does indeed appear to exist. This might serve to argue for H1 incorporation in regions which are still extended, but internal to the crystallites.)

The fact that annealing to $\sim 1500\,^{\circ}C$ is required before significant change in intensity or linewidth is observed in samples containing H1 reveals not only the high stability of the defect but also that of the nearby hydrogens that produce the linewidth. This would appear to rule out breadth contributions from nearby weakly bound hydrogen as has been reported to emerge from CVD diamond at $\sim 850\,^{\circ}C$.[23] The failure to see N^0 emerge upon annealing to these high temperatures is also significant. If it is directly passivated, it means a very high stability in its passivated form, an unusual situation for donor passivation in most semiconductors.[24–26] On the other hand, it follows naturally if its absence is due to compensation and H1 is the dominant compensation center.

Figure 2 suggests a systematic dependence of the two hydrogen-related signals and that of neutral nitrogen on hydrogen concentration, while little correlation is apparent in Table I for the neutral nitrogen signal itself with nitrogen concentration. The absence of the N^0 signal at high hydrogen concentration, even in samples with high nitrogen concentration, suggests either direct hydrogen passivation of the nitrogen donor (presumably substitutional nitrogen *is* present), or compensation by a deeper defect. In either case, the corresponding emergence of H1 at these high hydrogen concentrations suggests it to be electrically active, perhaps the compensating defect itself, with a double occupancy level below that of the nitrogen donor level at $E_c - 2.0$ eV,[27–29] which is EPR active only when singly occupied, i.e., with the Fermi level at or below its level. (In this model, the simultaneous presence of weaker N^0 and H1 signals in two of the samples of Table I and Fig. 2 at intermediate hydrogen concentrations could be the result of sample inhomogeneities.) The simultaneous presence of H2 and N^0 at low hydrogen concentration suggests the nonparamagnetic two-electron level of H2 to be above the nitrogen $E_c - 2.0$ eV donor level. Preliminary attempts to test these ideas by optical excitation *in situ* with ~ 15 mW of 325 nm light (3.8 eV) from a He-Cd laser produced no detectable changes of intensity for any of the three signals. This simple Fermi level argument therefore may or may not be correct. Further tests with higher energy near-band-gap light ($\geqslant 5.5$ eV) or ionization from an alternative source such as electron irradiation are planned.

We tentatively conclude therefore that H1 and H2 arise from two distinct electically active defects produced when a single hydrogen atom enters a stretched bond at a grain boundary, or other extended misfit region in the polycrystalline CVD material. In this model the hydrogen forms a bond with one of the carbons, producing an electrically active dangling bond on the other as the two carbons relax backward. Presumably hydrogen successfully passivates most of the many dangling bonds in such regions. However, in the particular cases of H1 and H2, hydrogen has either *activated* a stretched bond, or at least has failed to completely passivate it.

This behavior bears a close resemblance to recent observations in polycrystalline silicon, where strong evidence of hydrogen *activation* of grain boundaries has been presented. There too, the mechanism has been suggested to result from hydrogen entering a weak Si-Si bond at a grain boundary.[30–32] There, two different models have been suggested — (1) bond breaking and the production of a dangling bond,[30,32] as deduced here in diamond, or (2) the formation of bond-centered hydrogen, as is believed to occur for interstitial hydrogen in the perfect crystal, with similar electrical activity, which is not dangling-bondlike.[31] Our results in diamond serve to confirm the general concept of hydrogen entering a weak bond, but, at the same time, suggest that asymmetric relaxation to produce a single dangling bond may be the correct interpretation. (The hyperfine parameters anticipated for bond-centered hydrogen in diamond can be estimated by scaling the observed parameters for bond-centered interstitial muonium in diamond[9] by the ratio of the proton and muon free atom hyperfine interactions, as has been shown to be reliable for interstitial bond-centered hydrogen in silicon.[33] This predicts $a \cong -66$ MHz and $b \cong +60$ MHz, well out of the narrow allowable range required to match our spectra.)

Similar studies would be very difficult in polycrystalline silicon. There the hyperfine interaction would be smaller (inverse cube of interatomic separation) and the linewidths greater (angular average of the g-tensor anisotropy $\sim \lambda / E_g$) and it would be very unlikely therefore to find a microwave observation frequency where the forbidden transitions would be simultaneously intense enough and, at the same time, split out far enough to be observed. Indeed, a broad $g = 2.0055$ EPR center is observed in hydrogenated polycrystalline silicon that appears to correlate with hydrogen activation.[30,32] It appears indistinguishable, however, from the characteristic dangling bond center found in amorphous silicon, with no discernible satellite structure.[30,32] Diamond, therefore, with its smaller interatomic distances, its small spin-orbit interaction λ, and large band gap E_g, may indeed be unique in having offered us this opportunity to extract such detailed structural information on the role of hydrogen in producing electrical activity at stretched bonds in a diamond lattice semiconductor.

VI. SUMMARY

Two hydrogen-related defects, H1 and H2, have been observed by EPR in polycrystalline CVD diamond. H1, previously reported by several workers, is present primarily in high hydrogen-containing samples, where the isolated neutral nitrogen EPR signal is absent. For it, the relative intensities of its $\Delta m = \pm 1$ ''forbidden'' satellites reveal it to contain a single hydrogen atom ~ 1.9 Å away from the unpaired electron spin. H2, not previously reported, is observed only in lower hydrogen-containing samples, along with the neutral nitrogen signal, and the strength of its satellites indicates a similar center but with a single hydrogen ~ 2.3 Å away. These close distances have led us to propose that they arise when a single hydrogen atom enters a weak stretched C-C bond at a grain boundary, or other extended misfit region in the polycrystalline material, bonding to one carbon and activating the dangling bond of the other as the two carbons relax backward. These results may provide important insight

into the recently discovered phenomenon of hydrogen activation of grain boundaries in silicon, as well as its possible effect in other semiconductors.

ACKNOWLEDGMENTS

We are indebted to M. J. Stavola for critical comments and for pointing out to us the relevance of the work to the hydrogen activation problem in silicon. The EPR studies were performed at Lehigh University and were supported by the U. S. Office of Naval Research (Electronics and Solid State Sciences Program) under Grant No. N00014-94-1-0117. R.P.M. and S.C. would like to acknowledge the support, in part, by the Laboratory for Research on the Structure of Matter through NSF Grant No. DMR91-20668.

*Present address: Department of Chemical Engineering, Worcester Polytechnic Institute, Worcester, MA 01609.

†Present address: Department of Chemistry, University of Pennsylvania, Philadelphia, PA 19104.

[1] Ichiro Watanabe and Ken Sugata, Jpn. J. Appl. Phys. **27**, 1808 (1988).

[2] M. Fanciulli and T. D. Moustakas, Phys. Rev. B **48**, 14 982 (1993).

[3] H. Jia, J. Shinar, D. P. Lang, and M. Pruski, Phys. Rev. B **48**, 17 595 (1993).

[4] S. L. Holder, L. G. Rowan, and J. J. Krebs, Appl. Phys. Lett. **64**, 1091 (1994).

[5] M. Hoinkis, E. R. Weber, M. I. Landstrass, M. A. Piano, S. Han, and D. R. Kania, Appl. Phys. Lett. **59**, 1870 (1991).

[6] A. M. Portis, Phys. Rev. **91**, 1071 (1953).

[7] G. T. Trammell, H. Zeldes, and R. Livingston, Phys. Rev. **110**, 630 (1958).

[8] L. E. Halliburton, B. D. Perlson, R. A. Weeks, J. A. Weil, and M. C. Wintersgill, Solid State Commun. **30**, 575 (1979).

[9] B. D. Patterson, Rev. Mod. Phys. **60**, 69 (1988).

[10] G. D. Watkins and J. W. Corbett, Phys. Rev. **134**, A1359 (1964).

[11] E. L. Elkin and G. D. Watkins, Phys. Rev. **174**, 881 (1968).

[12] G. D. Watkins and J. W. Corbett, Phys. Rev. **138**, A543 (1965).

[13] M. J. S. Dewar *et al.*, J. Am. Chem. Soc. **107**, 3902 (1985).

[14] *Handbook of Gaussian Basis Sets*, edited by R. Poirier, R. Kari, and I. G. Csizmadia (Elsevier, Amsterdam, 1985).

[15] Gerhard Herzberg, *Infrared and Raman Spectra of Polyatomic Molecules,* Molecular Spectra and Molecular Structure, Vol. II (Van Nostrand, Princeton, NJ, 1945).

[16] Sanjay Chawla and Richard P. Messmer, J. Chem. Phys. **103**, 7442 (1995).

[17] D. M. Chipman, Theor. Chim. Acta. **76**, 73 (1989).

[18] C. Kittel and E. Abrahams, Phys. Rev. **90**, 238 (1953).

[19] J. H. Van Vleck, Phys. Rev. **74**, 1168 (1948).

[20] K. M. McNamara, B. E. Williams, K. K. Gleason, and B. E. Scruggs, J. Appl. Phys. **76**, 2466 (1994).

[21] D. H. Levy and K. K. Gleason, J. Phys. Chem. **96**, 8125 (1992).

[22] M. Pruski, D. P. Lang, Son-Jong Hwang, H. Jia, and J. Shinar, Phys. Rev. B **49**, 10 635 (1994).

[23] S. Mitra and K. K. Gleason, Diamond Related Mater. **2**, 126 (1993).

[24] J. Zhu, N. M. Johnson, and C. Herring, Phys. Rev. B **41**, 12 354 (1990).

[25] S. J. Pearton and J. Lopata, Appl. Phys. Lett. **59**, 2841 (1991).

[26] S. J. Pearton, C. R. Abernathy, and J. Lopata, Appl. Phys. Lett. **59**, 3571 (1991).

[27] R. G. Farrer, Solid State Commun. **7**, 685 (1969).

[28] L. A. Vermeulen and R. G. Farrer, Diamond Res. **18**, 62 (1965).

[29] W. J. P. van Enckevort and E. H. Versteegen, J. Phys. Condens. Matter **4**, 2361 (1992).

[30] H. Nickel, W. B. Jackson, and N. M. Jackson, Phys. Rev. Lett. **71**, 2733 (1993).

[31] N. H. Nickel, N. M. Johnson, and Chris G. Van de Walle, Phys. Rev. Lett. **72**, 3393 (1994).

[32] N. H. Nickel, N. M. Johnson, and W. B. Jackson, Appl. Phys. Lett. **62**, 3285 (1993).

[33] Yu. V. Gorelkinski and N. N. Nevinnyi, Physica B **170**, 155 (1991).